PHYSICAL REVIEW B **92**, 020101(R) (2015)

# Measurement of transverse hyperfine interaction by forbidden transitions

Mo Chen (陈墨),[1,2] Masashi Hirose,[1,3] and Paola Cappellaro[1,3,*]

[1]*Research Laboratory of Electronics, Massachusetts Institute of Technology, Cambridge, Massachusetts 02139, USA*

[2]*Department of Mechanical Engineering, Massachusetts Institute of Technology, Cambridge, Massachusetts 02139, USA*

[3]*Department of Nuclear Science and Engineering, Massachusetts Institute of Technology, Cambridge, Massachusetts 02139, USA*

(Received 14 April 2015; revised manuscript received 21 May 2015; published 6 July 2015)

Precise characterization of a system's Hamiltonian is crucial to its high-fidelity control that would enable many quantum technologies, ranging from quantum computation to communication and sensing. In particular, nonsecular parts of the Hamiltonian are usually more difficult to characterize, even if they can give rise to subtle but non-negligible effects. Here we present a strategy for the precise estimation of the transverse hyperfine coupling between an electronic and a nuclear spin, exploiting effects due to nominally forbidden transitions during the Rabi nutation of the nuclear spin. We applied the method to precisely determine the transverse coupling between a nitrogen-vacancy center electronic spin and its nitrogen nuclear spin. In addition, we show how this transverse hyperfine coupling, which has been often neglected in experiments, is crucial to achieving large enhancements of the nuclear Rabi nutation rate.

DOI: 10.1103/PhysRevB.92.020101 PACS number(s): 76.70.Hb, 03.67.Lx, 76.60.−k, 76.70.Dx

Quantum technologies promise to revolutionize many fields, ranging from precision sensing to fast computation. The success of novel technologies based on quantum effects rests on engineering quantum systems robust to noise and decoherence and on controlling them with high precision. Solid-state systems comprising nuclear spins have emerged as promising candidates, since the nuclear spin qubits are only weakly coupled to external fields and thus exhibit long coherence times. In order for nuclear spins to be used as good qubits, there are two important requirements: Their Hamiltonians need to be known with very high precision, as this would enable applying, e.g., optimal control methods [1,2], and strong driving should be available, in order to achieve fast gates. Here we show how to meet these two requirements by exploiting nominally forbidden transitions in a hybrid electronic-nuclear spin system associated with the nitrogen-vacancy center in diamond [3]. Specifically, we use second-order effects due to mixing of the electronic and nuclear spin states [4] in order to identify with high precision their coupling strength and to enhance the nuclear spin nutation rate [5].

The nitrogen-vacancy (NV) center is a naturally occurring point defect in diamond [6]. Owing to its optical properties and long coherence times, it has emerged as a versatile system for quantum sensing [7–9], quantum information [10,11], and photonics applications [12,13]. The nuclear $^{14}$N spin often plays an important role in these applications. Not only can it serve as a qubit in small quantum algorithms [14–16], but it can also be used to enhance the readout fidelity of the NV electronic spin [17] and achieve more sensitive detection of magnetic fields [18,19] and rotations [20,21]. These applications are made possible by the hyperfine interaction between the NV electronic and nuclear spins.

While the secular part of the NV-$^{14}$N Hamiltonian has been well characterized before [22–24], the transverse hyperfine coupling is more difficult to measure [25] and published values do not match well [26–28]. The most precise characterization to date has been achieved by ensemble electron spin resonance (ESR) techniques [27]. In that work, the ESR spectrum of an ensemble of NV centers was measured by induction methods while applying a magnetic field along the ⟨110⟩ direction to amplify nominally forbidden transitions. This method is not applicable to single NV centers, since the strong transverse field would quench the spin-dependent optical contrast.

Here we propose a different strategy to measure the transverse hyperfine coupling that can be carried out with optically detected magnetic resonance. Owing to this method we can determine the value of the transverse coupling with high precision. The method is not restricted to the NV spin system, but could be applied more generally to other electronic-nuclear spin systems, such as phosphorus [29] or antimony [30] donors in silicon, defects in silicon carbide [31,32], or quantum dots [33]. Precise knowledge of the hyperfine interaction tensor would enable achieving more precise control, elucidating modulations of the NV echo dynamics or, as we show here, achieving faster Rabi nutation of the nuclear spin.

*Theoretical model.* The NV ground state is a two-spin system given by the electronic spin of the NV center ($S = 1$) and the nuclear spin ($I = 1$) of the substitutional $^{14}$N adjacent to the vacancy that comprise the defect. In the experiments, we are only interested in two of the nuclear spin levels ($m_I = +1,0$) that we drive on resonance, while the third level can be neglected. Then, the Hamiltonian of the reduced system [34,35] is given by $\mathcal{H} = \mathcal{H}_\parallel + \mathcal{H}_\perp$, where the secular, $\mathcal{H}_\parallel$, and nonsecular, $\mathcal{H}_\perp$, terms are

$$\mathcal{H}_\parallel = \Delta S_z^2 + \left(\gamma_e B_z + \frac{A_\parallel}{2}\right) S_z + (Q + \gamma_n B_z) I_z + A_\parallel S_z I_z,$$
$$\mathcal{H}_\perp = \sqrt{2} A_\perp (S_x I_x + S_y I_y). \quad (1)$$

Here, $S$ and $I$ are the electron spin-1 and nuclear spin-1/2 operator, respectively. Also, $\Delta = 2.87$ GHz is the zero-field splitting and $Q = -4.945$ MHz [23] is the nuclear quadrupolar interaction. The NV spin is coupled to the nuclear spin by a hyperfine interaction with a longitudinal component $A_\parallel = -2.162$ MHz [23] and a transverse component $A_\perp$ which we

*pcappell@mit.edu

 

want to estimate. A magnetic field $B_z$ is applied along the NV crystal axis [111] to lift the degeneracy of the $m_s = \pm 1$ level, yielding the electron and nuclear Zeeman frequencies $\gamma_e B_z$ and $\gamma_n B_z$, where $\gamma_e = 2.8$ MHz/G and $\gamma_n = -0.308$ kHz/G.

Let $|m_s, m_I\rangle$ be eigenstates of $\mathcal{H}_\parallel$. The transverse coupling $A_\perp$ mixes states connected via zero-quantum (ZQ) transitions, $|+1,0\rangle \leftrightarrow |0,1\rangle$ and $|0,0\rangle \leftrightarrow |-1,1\rangle$. Diagonalization of the total Hamiltonian can then be achieved by rotating the two ZQ subspaces with a unitary transformation $U_{\mathrm{ZQ}} = e^{-i(\sigma_y^- \vartheta^- + \sigma_y^+ \vartheta^+)}$, where we defined $\sigma_y^+ = i(|+1,0\rangle\langle 0,1| - |0,1\rangle\langle +1,0|)$, $\sigma_y^- = i(|0,0\rangle\langle -1,1| - |-1,1\rangle\langle 0,0|)$, and the rotation angles are

$$\begin{aligned} \tan(2\vartheta^+) &= \frac{2A_\perp}{\Delta + \gamma_e B_z - \gamma_n B_z - Q}, \\ \tan(2\vartheta^-) &= \frac{-2A_\perp}{\Delta - \gamma_e B_z - A_\parallel + \gamma_n B_z + Q}. \end{aligned} \tag{2}$$

Because of this level mixing, a field on resonance with the nuclear spin transition also drives electronic transitions. Although the electronic spin state is unchanged to first order, as long as the mixing is small, the nominally forbidden transitions result in an enhancement of the nuclear state nutation frequency, as we explain below.

When applying a radio frequency (rf) field to drive the nuclear spin, the interaction Hamiltonian of the NV-$^{14}$N system with the rf field is

$$\mathcal{H}_{\mathrm{rf}}(t) = 2B_1 \cos(\omega t)(\gamma_e S_x + \sqrt{2}\gamma_n I_x), \tag{3}$$

where $B_1$ is the rf field strength. The Hamiltonian can be simplified by going into a rotating picture at the rf frequency $\omega$ and applying the rotating wave approximation (RWA) to obtain $\mathcal{H}_{\mathrm{rf}} = B_1(\gamma_e S_x + \sqrt{2}\gamma_n I_x)$. We note that since we might have $\gamma_e B_1 \gg \omega$, effects from the counterrotating fields, such as Bloch-Siegert shifts of the electronic energies, might be present. These effects were, however, negligible at the fields and Rabi strengths used in the experiments [34]. Transforming $\mathcal{H}_{\mathrm{rf}}$ with the unitary $U_{\mathrm{ZQ}}$ and denoting states and operators in the new frame by a caret, we obtain $\hat{\mathcal{H}}_{\mathrm{rf}} = U_{\mathrm{ZQ}}\mathcal{H}_{\mathrm{rf}}(t)U_{\mathrm{ZQ}}^\dagger = \mathcal{H}_n + \mathcal{H}_e$, with

$$\mathcal{H}_n = \sqrt{2}\gamma_n B_1(\alpha_1|\hat{1}\rangle\langle\hat{1}|_e + \alpha_0|\hat{0}\rangle\langle\hat{0}|_e + \alpha_{-1}|-\hat{1}\rangle\langle-\hat{1}|_e)\hat{I}_x. \tag{4}$$

Here, $\alpha_{m_s}$ denote the enhancement factors in each manifold of the NV spin,

$$\alpha_{+1} \approx 1 + \frac{\gamma_e}{\gamma_n}\frac{A_\perp}{\Delta + \gamma_e B_z - \gamma_n B_z - Q}, \tag{5}$$

$$\alpha_0 \approx 1 - \frac{\gamma_e}{\gamma_n}\left(\frac{A_\perp}{\Delta + \gamma_e B_z - \gamma_n B_z - Q} + \frac{A_\perp}{\Delta - \gamma_e B_z - A_\parallel + \gamma_n B_z + Q}\right), \tag{6}$$

$$\alpha_{-1} \approx 1 + \frac{\gamma_e}{\gamma_n}\frac{A_\perp}{\Delta - \gamma_e B_z - A_\parallel + \gamma_n B_z + Q}, \tag{7}$$

where we show expressions exact up to the first order in $\vartheta^\pm$ (see Ref. [34] for the exact expressions). The Hamiltonian $\mathcal{H}_e$ can be neglected since electronic spin transitions are far off resonance.

Owing to the strong dependence of the enhancement factors on the transverse hyperfine coupling, we can determine $A_\perp$ with high precision from measurement of the $^{14}$N Rabi oscillations.

*Experiments*. We used a home-built confocal microscope to measure the transverse hyperfine interaction of a single NV center in an electronic grade diamond sample (Element Six, $^{14}$N concentration $n_{\mathrm{N}} < 5$ ppb, natural abundance of $^{13}$C). The NV center is chosen to be free from close-by $^{13}$C. We worked at magnetic fields (300–500 G) close to the excited state level anticrossing so that during optical illumination at 532 nm, polarization of the NV spin can be transferred to the nuclear spin by their strong hyperfine coupling in the excited state [36]. As a result, a 1 $\mu$s laser excitation polarizes the NV-$^{14}$N system into the $|0,1\rangle$ state.

Then, the NV spin is prepared in the desired Zeeman state by a strong microwave (MW) pulse ($t_p \approx 50$ ns) before coherently driving the nuclear spin by an rf field on resonance with the nuclear transition $|m_s,1\rangle \leftrightarrow |m_s,0\rangle$, for a duration $\tau$ (see Fig. 1). Finally, the nuclear spin state is detected by employing a MW selective pulse ($t_p \approx 700$ ns) that maps the nuclear spin state onto the NV spin, which in turn can be read out optically due to spin-dependent fluorescence emission intensity. The nuclear Rabi oscillations in Fig. 2 clearly show that for a fixed driving strength, the effective Rabi frequency is quite different in the three electronic spin manifolds.

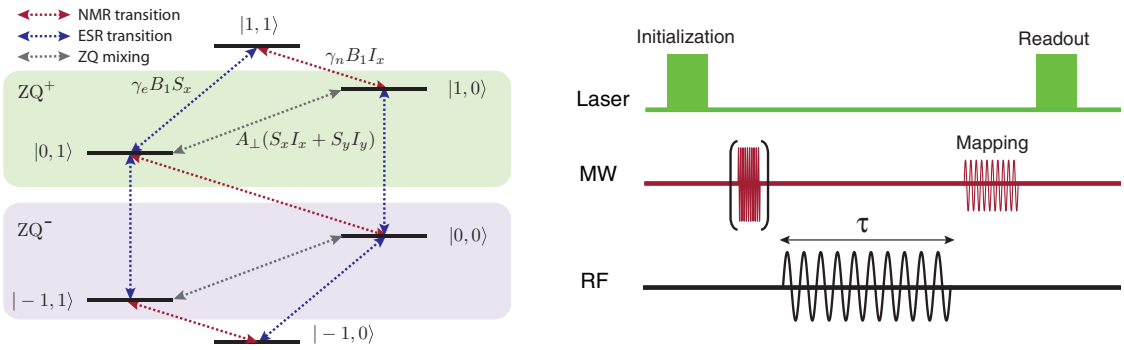


FIG. 1. (Color online) Left: Energy levels of the reduced NV-$^{14}$N spin system, showing the transitions that are mixed by transverse hyperfine coupling. Right: Experimental sequence used to measure the nuclear $^{14}$N Rabi frequency in the three NV manifolds.

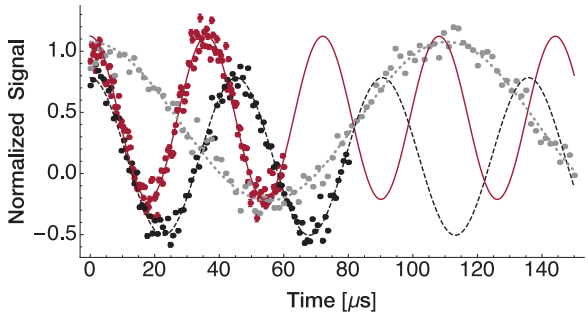


FIG. 2. (Color online) $^{14}$N Rabi oscillations at $B = 450$ G, $B_1 \approx 3.3$ G in the three NV manifolds (red solid line, $m_s = 0$; black dashed line, $m_s = -1$; gray dotted line, $m_s = +1$). Here, the dots are the experimental results, while the lines are fits to cosine oscillations. The different baseline of the $m_s = -1$ curve is due to small differences in the fluorescence emission of different nuclear manifolds [36].

To confirm the expected dependence of the Rabi enhancement factors on the external magnetic field and the NV state, we measured the Rabi oscillations at the three electronic spin manifolds with varying magnetic field $B_z$. As shown in Fig. 3, the measured Rabi frequencies match well with the theoretical model. It is worth noting that contrary to the static pseudonuclear Zeeman effect [4], there is a large enhancement ($\alpha_0 \approx 16$, $\alpha_{\pm 1} \approx -9$) even at zero field. Also, close to the ground state avoided crossing ($B \approx 0.1$ T), the enhancement can become very large, exceeding 100. The validity of our approximation in this regime can be confirmed by numerical simulations [34].

While these experiments could be used to extract $A_\perp$, this is not a practical method to obtain a good enough estimate. The range of magnetic field is restricted by the need to be close to the excited state level anticrossing to achieve a good polarization of the nuclear spin. The number of acquired points is limited by the time it takes to change and properly align the external magnetic field. In addition, there might be variations

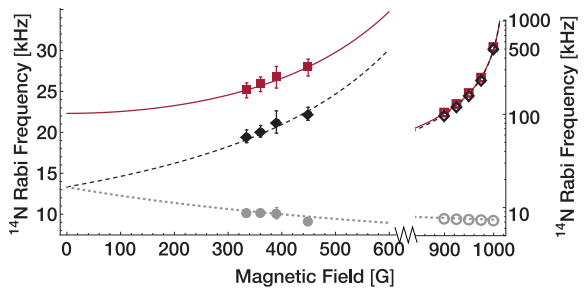


FIG. 3. (Color online) $^{14}$N Rabi frequency in the three NV manifold (red solid line, $m_s = 0$; black dashed line, $m_s = -1$; gray dotted line $m_s = +1$) as a function of the magnetic field. Rabi frequency corresponds to $\frac{\gamma_n B_1}{\sqrt{2}\pi}\alpha_{m_s}$. The solid symbols correspond to the experimental data, which match closely the theoretical prediction. The effective Rabi frequencies increase rapidly with the field, exceeding 1 MHz when close to the ground state level anticrossing. The enhancement allows fast manipulation of the nuclear spin even when the bare Rabi field is only $B_1 \approx 3.3$ G. The theoretical prediction is confirmed by simulations (open symbols) of the spin dynamics.

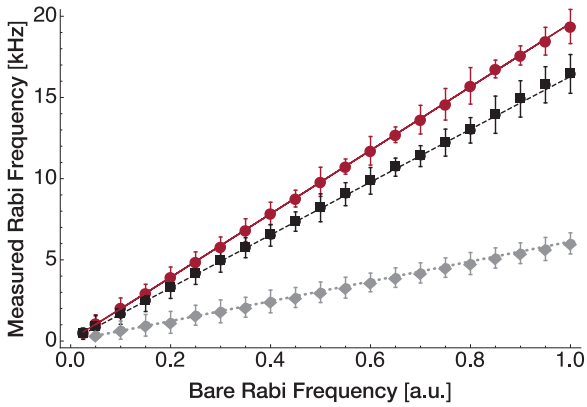


FIG. 4. (Color online) Measured enhanced $^{14}$N Rabi frequency in the three NV manifolds (red solid line, $m_s = 0$; black dashed line, $m_s = -1$; gray dotted line $m_s = +1$) as a function of the bare Rabi frequency at $B = 509$ G.

in the bare Rabi frequency in the three manifolds, because of different responses of the electronics used to drive the nuclear spins at the different frequencies.

In order to avoid these difficulties, we fixed the magnetic field to 509 G and instead linearly swept the amplitude of the rf driving ($B_1$). With this procedure, we do not need an independent measure of the bare Rabi frequency in order to extract the transverse hyperfine coupling strength. The relative rf amplitudes $B_1$ obtained when varying the driving strength can be measured at each nuclear resonance frequency by monitoring the rf voltage with an oscilloscope, confirming its linear dependence with applied power.

We thus measure the effective nuclear Rabi frequency as a function of the normalized rf amplitude $B_1/|B_{1,\max}|$ in all three electronic manifolds (Fig. 4). The measured Rabi frequency $\Omega_m$ is related to its on-resonance value by $\Omega_m = \sqrt{\Omega^2 + \delta^2}$, where $\delta$ is the detuning from the nuclear spin resonance frequency. We incorporate this unknown, small detuning in our model and fit the experimental data with the Rabi enhancement formulas (5)–(7). From the fit, we obtain an estimate of the transverse hyperfine coupling, $A_\perp = -2.62 \pm 0.05$ MHz, in good agreement with recently published values and with better precision.

In order to achieve even better precision, we need to consider all the sources of uncertainty and errors. We find that small errors from imperfect MW $\pi$ pulses and nuclear polarization only contribute to a reduced fluorescent contrast, but do not affect the estimate of the Rabi frequency under our experimental condition. The detuning of the selective MW and rf pulses from resonance and uncertainty in $A_\parallel$ contributes only linearly to the uncertainty. All these minor errors and uncertainties hardly affect the final uncertainty in the estimate of $A_\perp$ [34]. The major source of error arises instead from the uncertainty in the measured Rabi frequency, which is limited by the photon shot noise of the optical readout process. Therefore, the precision of the estimate could be improved with more averaging, at the expense of a longer measurement time. Currently, our total measurement time is limited by the stability of the experimental setup, yielding $\delta A_\perp \sim 50$ kHz. Improving the stability of the setup by reducing thermal fluc-

tuations and noise in the driving field (also using decoupling schemes [37,38]), or by employing small ensembles or more efficient optical readout methods such as solid-immersion lenses [39] and charge-state sensing [40], could provide higher precision. Then, the limit would come from uncertainties in $\gamma_e$ and $\gamma_n$, with a relative error of $10^{-4}$ [26,41], yielding an uncertainty in $A_\perp$ of a few hundred Hz [34].

*Conclusions*. In conclusion, we observed enhanced nuclear Rabi oscillations in the NV-$^{14}$N system due to level mixing between electronic and nuclear spin states. We harness the strong dependence of this enhancement on the transverse hyperfine coupling to determine its value with high precision. Theoretical analysis predicts an enhancement factor of almost three orders of magnitude when the magnetic field is close to the ground state level anticrossing, promising fast manipulation of the nuclear spin qubit at ∼MHz rates, with only moderate driving strengths. More broadly, the method presented here can be applied to many other electron-nuclear hybrid spin systems to similarly characterize their interaction Hamiltonian with high precision. Our results indicate that taking into account the nonsecular parts of a system's Hamiltonian is crucial to achieving faster and more accurate control of the quantum system.

This work was supported in part by the U.S. Air Force Office of Scientific Research Grant No. FA9550-12-1-0292 and by the U.S. Office for Naval Research Grant No. N00014-14-1-0804.

M.C. and M.H. contributed equally to this work.

[1] N. Khaneja, T. Reiss, C. Kehlet, T. Schulte-Herbuggen, and S. Glaser, J. Magn. Reson. **172**, 296 (2005).

[2] J. Scheuer, X. Kong, R. S. Said, J. Chen, A. Kurz, L. Marseglia, J. Du, P. R. Hemmer, S. Montangero, T. Calarco, B. Naydenov, and F. Jelezko, New J. Phys. **16**, 093022 (2014).

[3] A. Gruber, A. Drabenstedt, C. Tietz, L. Fleury, J. Wrachtrup, and C. v. Borczyskowski, Science **276**, 2012 (1997).

[4] A. Abragam and B. Bleaney, *Electron Paramagnetic Resonance of Transition Ions* (Clarendon, Oxford, UK, 1970).

[5] S. Sangtawesin and J. R. Petta, arXiv:1503.07464.

[6] *The Properties of Natural and Synthetic Diamond*, edited by J. E. Field (Academic, London, 1992).

[7] J. M. Taylor, P. Cappellaro, L. Childress, L. Jiang, D. Budker, P. R. Hemmer, A. Yacoby, R. Walsworth, and M. D. Lukin, Nat. Phys. **4**, 810 (2008).

[8] F. Dolde, H. Fedder, M. W. Doherty, T. Nobauer, F. Rempp, G. Balasubramanian, T. Wolf, F. Reinhard, L. C. L. Hollenberg, F. Jelezko, and J. Wrachtrup, Nat. Phys. **7**, 459 (2011).

[9] D. M. Toyli, C. F. de las Casas, D. J. Christle, V. V. Dobrovitski, and D. D. Awschalom, Proc. Natl. Acad. Sci. USA **110**, 8417 (2013).

[10] J. Wrachtrup, S. Kilin, and A. Nizovtsev, Opt. Spectrosc. **91**, 429 (2001).

[11] P. Cappellaro, L. Jiang, J. S. Hodges, and M. D. Lukin, Phys. Rev. Lett. **102**, 210502 (2009).

[12] I. Aharonovich, A. D. Greentree, and S. Prawer, Nat. Photonics **5**, 397 (2011).

[13] B. J. M. Hausmann, B. Shields, Q. Quan, P. Maletinsky, M. McCutcheon, J. T. Choy, T. M. Babinec, A. Kubanek, A. Yacoby, M. D. Lukin, and M. Loncar, Nano Lett. **12**, 1578 (2012).

[14] G. D. Fuchs, G. Burkard, P. V. Klimov, and D. D. Awschalom, Nat. Phys. **7**, 789 (2011).

[15] G. Waldherr, P. Neumann, S. F. Huelga, F. Jelezko, and J. Wrachtrup, Phys. Rev. Lett. **107**, 090401 (2011).

[16] R. E. George, L. M. Robledo, O. J. E. Maroney, M. S. Blok, H. Bernien, M. L. Markham, D. J. Twitchen, J. J. L. Morton, G. A. D. Briggs, and R. Hanson, Proc. Natl. Acad. Sci. USA **110**, 3777 (2013).

[17] P. Neumann, J. Beck, M. Steiner, F. Rempp, H. Fedder, P. R. Hemmer, J. Wrachtrup, and F. Jelezko, Science **329**, 542 (2010).

[18] E. M. Kessler, I. Lovchinsky, A. O. Sushkov, and M. D. Lukin, Phys. Rev. Lett. **112**, 150802 (2014).

[19] G. Arrad, Y. Vinkler, D. Aharonov, and A. Retzker, Phys. Rev. Lett. **112**, 150801 (2014).

[20] M. P. Ledbetter, K. Jensen, R. Fischer, A. Jarmola, and D. Budker, Phys. Rev. A **86**, 052116 (2012).

[21] A. Ajoy and P. Cappellaro, Phys. Rev. A **86**, 062104 (2012).

[22] M. Steiner, P. Neumann, J. Beck, F. Jelezko, and J. Wrachtrup, Phys. Rev. B **81**, 035205 (2010).

[23] B. Smeltzer, J. McIntyre, and L. Childress, Phys. Rev. A **80**, 050302 (2009).

[24] C. S. Shin, M. C. Butler, H.-J. Wang, C. E. Avalos, S. J. Seltzer, R.-B. Liu, A. Pines, and V. S. Bajaj, Phys. Rev. B **89**, 205202 (2014).

[25] J. G. Kempf and D. P. Weitekamp, J. Vac. Sci. Technol. B **18**, 2255 (2000).

[26] M. W. Doherty, N. B. Manson, P. Delaney, F. Jelezko, J. Wrachtrup, and L. C. Hollenberg, Phys. Rep. **528**, 1 (2013).

[27] S. Felton, A. M. Edmonds, M. E. Newton, P. M. Martineau, D. Fisher, D. J. Twitchen, and J. M. Baker, Phys. Rev. B **79**, 075203 (2009).

[28] X.-F. He, N. B. Manson, and P. T. H. Fisk, Phys. Rev. B **47**, 8816 (1993).

[29] J. J. L. Morton, A. M. Tyryshkin, R. M. Brown, S. Shankar, B. W. Lovett, A. Ardavan, T. Schenkel, E. E. Haller, J. W. Ager, and S. A. Lyon, Nature (London) **455**, 1085 (2008).

[30] G. Wolfowicz, M. Urdampilleta, M. L. W. Thewalt, H. Riemann, N. V. Abrosimov, P. Becker, H.-J. Pohl, and J. J. L. Morton, Phys. Rev. Lett. **113**, 157601 (2014).

[31] M. Widmann, S.-Y. Lee, T. Rendler, N. T. Son, H. Fedder, S. Paik, L.-P. Yang, N. Zhao, S. Yang, I. Booker, A. Denisenko, M. Jamali, S. A. Momenzadeh, I. Gerhardt, T. Ohshima, A. Gali, E. Janzén, and J. Wrachtrup, Nat. Mater. **14**, 164 (2015).

[32] A. L. Falk, P. V. Klimov, V. Ivády, K. Szász, D. J. Christle, W. F. Koehl, Á. Gali, and D. D. Awschalom, Phys. Rev. Lett. **114**, 247603 (2015).

[33] E. A. Chekhovich, M. N. Makhonin, A. I. Tartakovskii, A. Yacoby, H. Bluhm, K. C. Nowack, and L. M. K. Vandersypen, Nat. Mater. **12**, 494 (2013).

[34] See Supplemental Material at http://link.aps.org/supplemental/10.1103/PhysRevB.92.020101 for technical details of the theoretical model and error analysis.

[35] B. Bleaney, in *Hyperfine Interactions*, edited by A. Freeman and R. Frankel (Academic Press, London, 1967).

[36] V. Jacques, P. Neumann, J. Beck, M. Markham, D. Twitchen, J. Meijer, F. Kaiser, G. Balasubramanian, F. Jelezko, and J. Wrachtrup, Phys. Rev. Lett. **102**, 057403 (2009).

[37] J.-M. Cai, B. Naydenov, R. Pfeiffer, L. P. McGuinness, K. D. Jahnke, F. Jelezko, M. B. Plenio, and A. Retzker, New J. Phys. **14**, 113023 (2012).

[38] C. D. Aiello, M. Hirose, and P. Cappellaro, Nat. Commun. **4**, 1419 (2013).

[39] L. Marseglia, J. P. Hadden, A. C. Stanley-Clarke, J. P. Harrison, B. Patton, Y.-L. D. Ho, B. Naydenov, F. Jelezko, J. Meijer, P. Dolan, J. Smith, J. Rarity, and J. O'Brien, Appl. Phys. Lett. **98**, 133107 (2011).

[40] B. J. Shields, Q. P. Unterreithmeier, N. P. de Leon, H. Park, and M. D. Lukin, Phys. Rev. Lett. **114**, 136402 (2015).

[41] P. Neumann, Ph.D. thesis, University of Stuttgart, 2012.

# Measurement of transverse hyperfine interaction by forbidden transitions

## Supplementary Material

Mo Chen (陈墨), [1,2,*] Masashi Hirose, [1,3,*] and Paola Cappellaro[1,3,†]

[1]Research Laboratory of Electronics, Massachusetts Institute of Technology, Cambridge, MA 02139, USA
[2]Department of Mechanical Engineering, Massachusetts Institute of Technology, Cambridge, MA 02139, USA
[3]Department of Nuclear Science and Engineering, Massachusetts Institute of Technology, Cambridge, MA 02139, USA

## 1 Exact expressions for the Rabi enhancement

### 1.1 NV center system

For single NV, we effectively polarize the nitrogen nuclear spin at +1 (around excited state level anti-crossing $\sim 500$G), and the only transition of concern is $|m_I = +1\rangle \leftrightarrow |m_I = 0\rangle$. We simplify the problem by reducing nuclear spin-1 to an effective spin-1/2 system by applying the following transform where a factor of $\sqrt{2}$ is introduced

$$I_z^2, I_z \to \frac{1}{2}\mathbb{1} + I_z, \qquad I_{x,y} \to \sqrt{2} I_{x,y} \tag{1}$$

In the main text we described our procedure to find expression for the enhancement of the nuclear spin Rabi nutation due to virtual transitions of the electronic spin. Here we provide the exact expressions for the enhancement factor in each electronic spin manifold $m_s$:

$$\begin{aligned} \alpha_{+1} &= \cos(\vartheta^+) + \frac{\gamma_e}{\gamma_n}\sin(\vartheta^+), \\ \alpha_0 &= \cos(\vartheta^+)\cos(\vartheta^-) - \frac{\gamma_e}{\gamma_n}\sin(\vartheta^+ - \vartheta^-), \\ \alpha_{-1} &= \cos(\vartheta^-) - \frac{\gamma_e}{\gamma_n}\sin(\vartheta^-). \end{aligned} \tag{2}$$

where the rotation angles, as shown in main text, are given by

$$\tan(2\vartheta^+) = \frac{2A_\perp}{\Delta + \gamma_e B_z - \gamma_n B_z - Q} = \frac{2A_\perp}{\omega_{\rm mw}^{+1} - \omega_{\rm rf}^{+1}}, \tag{3}$$

$$\tan(2\vartheta^-) = \frac{-2A_\perp}{\Delta - \gamma_e B_z - A_\parallel + \gamma_n B_z + Q} = \frac{-2A_\perp}{\omega_{\rm mw}^{-1} + \omega_{\rm rf}^{-1} + A_\parallel}. \tag{4}$$

Here

$$\begin{aligned} \omega_{\rm mw}^{+1} &= \Delta + \gamma_e B_z + A_\parallel, \\ \omega_{\rm rf}^{+1} &= Q + \gamma_n B_z + A_\parallel, \\ \omega_{\rm mw}^{-1} &= \Delta - \gamma_e B_z - A_\parallel, \\ \omega_{\rm rf}^{-1} &= Q + \gamma_n B_z - A_\parallel. \end{aligned} \tag{5}$$

are the resonance frequencies for electron $|0, +1\rangle \leftrightarrow |\pm 1, +1\rangle$ and nuclear $|\pm 1, 1\rangle \leftrightarrow |\pm 1, 0\rangle$ transitions, which can be easily obtained experimentally.

Taking the approximation up to first order, we obtain equations linear in $A_\perp$ as given in the main text.

### 1.2 Electronic Spin-1/2

Formulas for the enhancement of the driving frequency when the nuclear spin is coupled to an electronic spin 1/2 have been reported previously [1]. For completeness, we provide here their expressions with the same

*These authors contributed equally to this work.
†pcappell@mit.edu

notations and derivation procedure as above. The system can be subdivided in two manifolds (a double-quantum and a zero-quantum manifold, where the mixing between nuclear and electronic transitions can occur). Following a procedure analogous to what described in the main text, we can rotate the ZQ manifold and thus obtained the enhancement factors:

$$\begin{aligned} \alpha_{+1/2} &= \cos(\vartheta) + \tfrac{\gamma_e}{\gamma_n}\sin(\vartheta), \\ \alpha_{-1/2} &= \cos(\vartheta) - \tfrac{\gamma_e}{\gamma_n}\sin(\vartheta). \end{aligned} \tag{6}$$

where the rotation angle $\vartheta$ is given by

$$\tan(2\vartheta) = \frac{\sqrt{2}A_\perp}{\gamma_e B_z - \gamma_n B_z - Q + \frac{A_\parallel}{2}} = \frac{\sqrt{2}A_\perp}{\omega_{\rm mw} - \omega_{\rm rf}}, \tag{7}$$

with

$$\omega_{\rm mw} = \gamma_e B_z, \qquad \omega_{\rm rf} = \gamma_n B_z + Q - \frac{A_\parallel}{2}. \tag{8}$$

Note that for a nuclear spin 1/2, the same formulas are valid with the replacement $\omega_{\rm rf} = \gamma_n B_z$ and replace $\sqrt{2}A_\perp$ with $A_\perp$.

## 2 Validity of Rabi enhancement formulas

In order to obtain the expressions in Eq. (2), we made some approximations; in particular we neglected the counter-rotating term of the RF driving field and, after the diagonalization procedure presented in the main text, we neglect any off-resonance transition involving electronic spin levels. Since for the electronic spin the driving field strength $\gamma_e B_1$ is typically much larger than the driving frequency $\omega_{\rm rf}$, the first approximation might not always hold.

To test the validity of these approximations and thus of our enhancement formulas Eq. (2), we performed numerical simulation using a first-order Trotter expansion in the lab frame, thus considering both rotating and counter-rotating terms. Here we used the same parameters as in the experiments. Figure 1 shows a good agreement between Trotter simulation and our theoretical formula, even for very large RF strength. This indicates that although the nominal bound for the validity of the rotating wave approximation (RWA) for the electronic spin might be broken, its effects on the nuclear spin transitions are small. From these results we conclude that for the RF strengths used in our experiment, effects from counter-rotating fields and other approximations are on the order of $10^{-4}$ of Rabi nutation rate, two orders of magnitude smaller than our estimated uncertainty $\delta A_\perp$ and thus do not affect our estimate of the value of $A_\perp$.

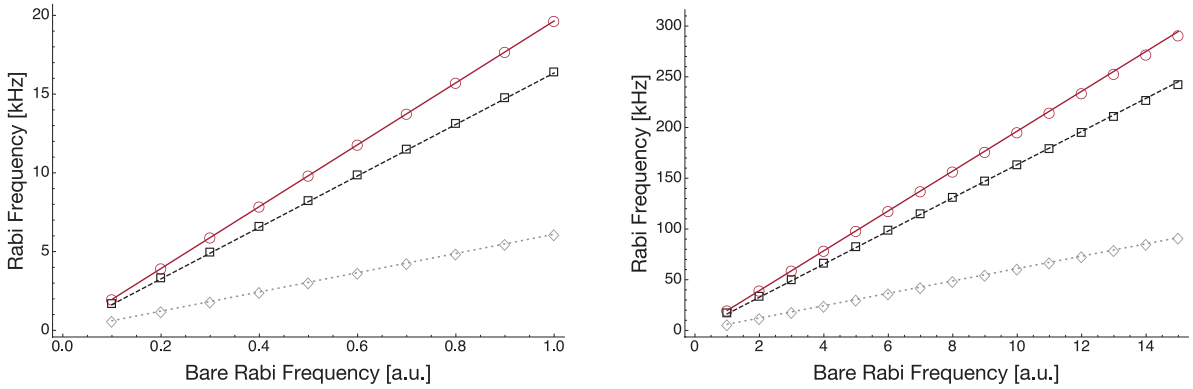


Figure 1: Left: Comparison between theoretical formula (lines) and Trotter simulation (open symbols). Red, circles, $m_s = 0$. Black (dashed line and squares), $m_s = -1$. Gray (dotted line and diamonds), $m_s = +1$. This range corresponds to our experimental condition, where RWA is shown valid. Relative error between Trotter and theoretical curve is $\sim 10^{-4}$. Right: Comparison between theoretical formula (solid line) and trotter simulation (open symbols) over large range of RF strength. Red, $m_s = 0$. Black, $m_s = -1$. Gray, $m_s = +1$. Good agreement indicates small effects from counter-rotating term.

## 3 Error Analysis

In the main text, when discussing the uncertainty in the estimate of $A_\perp$, resulting from our measurement and fitting procedure, we only considered error from measured nuclear Rabi frequency. For a comprehensive discussion of error, we need to consider all the sources of uncertainty and errors.

Small errors from imperfect MW $\pi$ pulses duration and nuclear spin polarization contribute to reduction of fluorescent contrast and do not enter our estimation procedure. Under current experimental conditions, these two factors are negligible. The detuning of selective MW pulse is estimated by measuring the linewidth of fourier transformed electronic spin Ramsey signal. To find the uncertainty in RF frequency, we perform pulsed RF excitation, sweeping across the resonance frequency and observing the fluorescence intensity after mapping the nuclear spin state to the electronic spin. The linewidth of the observed dip provides us a conservative estimate of the uncertainty in $\omega_{\rm rf}$. These uncertainties range from $1.8-7.9$ kHz. In the fitting process, uncertainty in $A_\parallel$ also contributes linearly. It was measured with high precision before [2].

In the estimation procedure, we truncate Eq.(2) to first order and rewrite them in order to express $A_\perp$ as a function of experimental measurements:

$$\begin{aligned} A_\perp &= \frac{\gamma_n}{\gamma_e}(\omega_{\rm mw}^{+1}-\omega_{\rm rf}^{+1})(\frac{\pi\Omega_{+1}}{\gamma_n B_1}-1) \\ &= \frac{\gamma_n}{\gamma_e}(\omega_{\rm mw}^{-1}+\omega_{\rm rf}^{-1}+A_\parallel)(\frac{\pi\Omega_{-1}}{\gamma_n B_1}-1) \\ &= \frac{\gamma_n}{\gamma_e}(\frac{1}{\omega_{\rm mw}^{+1}-\omega_{\rm rf}^{+1}}+\frac{1}{\omega_{\rm mw}^{-1}+\omega_{\rm rf}^{-1}+A_\parallel})^{-1}(1-\frac{\pi\Omega_0}{\gamma_n B_1}) \end{aligned} \tag{9}$$

We calculate contributions to the uncertainty $\delta A_\perp$ of $A_\perp$ from all fitting parameters using the approximate propagation of error formula, $\delta A_\perp(x_1,x_2,\cdots)=\sqrt{\Sigma_n\left(\frac{\partial A_\perp}{\partial x_n}\right)^2\delta x_n^2}$. The contribution of each factor, $D_x=|\frac{\partial A_\perp}{\partial x}\delta x|$, calculated according to Eq. 9 using values from our experiment are reported in Table 1.

These results show that uncertainties from $\omega_{\rm mw}$, $\omega_{\rm rf}$ and $A_\parallel$ are at least 4 orders smaller than that from the measured nuclear Rabi frequency $\Omega_{m_s}$. Therefore, our fitting considering only error from measured Rabi frequency is valid.

The uncertainty in the Rabi frequency is limited by coherence time of the nuclear spin under driving (which can introduce further decoherence due to the driving field instability) and photon shot noise of the optical readout process. Thus the precision of the estimate could be improved with more averaging, at the expense of longer measurement time, or by using more advanced readout techniques [3, 4]. Another limit of a few hundred Hz is imposed by accuracy of $\gamma_e$ and $\gamma_n$, with $\sim 10^{-4}$ relative error [5, 6].

| | $\delta\omega_{\rm mw}$ | $D_{\omega_{\rm mw}}$ | $\delta\omega_{\rm rf}$ | $D_{\omega_{\rm rf}}$ | $\delta\Omega_{m_s}$ | $D_{\Omega_{m_s}}$ | $\delta A_\parallel$ | $D_{A_\parallel}$ (Hz) |
|---|---|---|---|---|---|---|---|---|
| $m_s=+1$ | $5.5\times10^3$ | 3 | $1.8\times10^3$ | 1 | 650 | $2.7\times10^5$ | $2\times10^3$ | 0 |
| $m_s=0$ | — | 8* | — | 11* | $1\times10^3$ | $1.3\times10^5$ | $2\times10^3$ | 3 |
| $m_s=-1$ | $5.5\times10^3$ | 10 | $7.9\times10^3$ | 14 | $1\times10^3$ | $1.6\times10^5$ | $2\times10^3$ | 4 |

Table 1: Contribution to uncertainty in $A_\perp$ from all parameters according to Eq. (9) and the error propagation formula. $D_x$ stands for $|\frac{\partial A_\perp}{\partial x}\delta x|$.

*In the electronic $m_s=0$ manifold, $\omega_{\rm mw}^0$ and $\omega_{\rm rf}^0$ do not enter Eq. (9), while $\omega_{\rm mw}^{\pm1}$ and $\omega_{\rm rf}^{\pm1}$ contribute. The error is estimated by combining contributions from the $m_s=\pm1$ manifolds, $D_{\omega,0}=\sqrt{D_{\omega,+1}^2+D_{\omega,-1}^2}$.

## References


[1] Bleaney, in *Hyperfine interactions*, edited by A. Freeman and R. Frankel (Academic Press, 1967) p. 1.

[2] B. Smeltzer, J. McIntyre, and L. Childress, Phys. Rev. A **80**, 050302 (2009).

[3] L. Marseglia, J. P. Hadden, A. C. Stanley-Clarke, J. P. Harrison, B. Patton, Y.-L. D. Ho, B. Naydenov, F. Jelezko, J. Meijer, P. Dolan, J. Smith, J. Rarity, and J. OBrien, Appl. Phys. Lett. **98**, 133107 (2011).

[4] B. J. Shields, Q. P. Unterreithmeier, N. P. de Leon, H. Park, and M. D. Lukin, Phys. Rev. Lett. **114**, 136402 (2015).

[5] M. W. Doherty, N. B. Manson, P. Delaney, F. Jelezko, J. Wrachtrup, and L. C. Hollenberg, Physics Reports **528**, 1 (2013).

[6] P. Neumann, *Towards a room temperature solid state quantum processor—The nitrogen-vacancy center in diamond*, Ph.D. thesis, University of Stuttgart (2012).